Progress In Electromagnetics Research B, Vol. 116, 94–106, 2026

PIER B

(Received 13 October 2025, Accepted 9 December 2025, Scheduled 1 January 2026)

Microstrip Array Antenna Design for a 24 GHz Radar-Based Vital Signs Monitoring System

Murtini Murtini[1], Nurhayati Nurhayati[1,*], Usman R. Iman[2],
Fitri Y. Zulkifli[3], Dewiani Dewiani[4], and Lilik Anifah[1]

[1]*Department of Electrical Engineering, Universitas Negeri Surabaya, Surabaya 60231, Indonesia*
[2]*Department of Electronic Engineering, Hanyang University, Seoul 04763, South Korea*
[3]*Department of Electrical Engineering, Universitas Indonesia, Depok 16435, Indonesia*
[3]*Departement of Electrical Engineering, Faculty of Engineering, Universitas Hasanuddin Gowa, South Sulawesi, Indonesia*

ABSTRACT: Non-contact vital sign monitoring using radar technology has become increasingly important in modern healthcare, as it enables continuous physiological measurements without direct contact with the skin, minimizing patient discomfort and the risk of infection. To address this need, this study presents the design and analysis of a 24 GHz microstrip antenna array developed for a radar-based vital sign monitoring system. Array configurations consisting of one to five circular patch elements were analyzed to optimize the reflection coefficient, directivity, and radiation characteristics, with the aim of achieving high sensitivity, compactness, and safety for biomedical radar applications. Simulation results show that the four-element array achieves optimal performance, with a reflection coefficient of -39.27 dB, directivity of 5.29 dBi, and a bandwidth of 1.35 GHz at 24 GHz. To evaluate electromagnetic safety, Specific Absorption Rate (SAR) analysis using a three-layer human tissue model (skin, fat, and muscle) resulted in values of 0.159 W/kg (1 g) and 0.022 W/kg (10 g), both within ICNIRP and FCC limits. Additionally, bending simulations with a radius of curve at 10 mm, 20 mm, 30 mm and 40 mm showed stable impedance matching and minimal frequency variation, demonstrating high mechanical flexibility. On the whole, the proposed antenna exhibits high gain, reliable performance, and safety compliance, making it suitable for integration into portable radar-based medical devices for continuous, contactless monitoring of heart rate and respiration.

1. INTRODUCTION

Monitoring vital signs, especially heart rate, has an important role in the early detection and diagnosis of various cardiovascular conditions [1]. Conventional methods such as electrocardiography (ECG) [2], photoplethysmography (PPG) [3], phonocardiography (PCG) [4], impedance cardiography (ICG) [5], and ultrasound cardiography (UCG) [6] have long been used in cardiac monitoring systems. In general, these devices work by direct contact with the skin, so the measurement probe must be physically attached to the patient. This condition can limit movement and cause discomfort, especially in long-term monitoring.

As a solution to these limitations, radar systems have been developed for non-contact heart rate detection. Radar technology enables heart rate monitoring by relying on small changes on the body surface caused by heart and respiratory activity [7]. Several radar approaches used include frequency-modulated continuous wave (FMCW) [8], ultra-wideband (UWB) [9], continuous wave (CW) [10], and self-injection locking (SIL) [11].

To improve the performance of radar systems in vital sign monitoring, the use of a 24 GHz frequency is a promising option, as described in [12] and [13]. Previous research [14] shows that the 24 GHz frequency has better resolution in detecting micro-movements compared to lower frequencies, and allows for smaller antenna sizes, making it easier to integrate into radar-based medical monitoring systems [15]. Heartbeat signals have smaller amplitudes than breathing [16], so a system with high sensitivity and good spatial resolution capabilities is required.

Several recent designs use advanced structures to improve antenna gain and directivity, such as complementary split ring resonators (CSRRs) in the study [17]. In the study [18], fractal geometry has been successfully applied to medical imaging antennas to improve gain and reduce side lobe levels, contributing to better detection performance in biological applications.

Although various studies have examined the use of radar and antennas at 24 GHz and other bands for vital sign monitoring, there are still a number of limitations. A study in [19] proposed a 24 GHz flexible antenna for heart rate and respiration detection, but did not include Specific Absorption Rate (SAR) analysis or radiation pattern optimization using more complex arrays. Research [20] developed a wearable 24 GHz antenna for navigation applications, but did not focus on medical applications. Meanwhile, research [21] demonstrated the effectiveness of millimeter wave (mmWave) radar in the 76–81 GHz frequency range for vital sign monitoring, but did not investigate compact and economical antenna designs in the 24 GHz frequency range.

Recent work [22] emphasized the importance of SAR analysis and bending performance in wearable antenna applications,

* Corresponding author: Nurhayati Nurhayati (nurhayati@unesa.ac.id).

demonstrating that antenna flexibility, radiation pattern control, and substrate selection directly affect both electromagnetic safety and data transmission quality in health monitoring systems. However, despite these advances, there remains limited research specifically focused on optimizing 24 GHz microstrip array antennas for radar-based medical monitoring, integrating both high-performance design and user safety aspects.

The novelty and main contributions of this research are summarized as follows:

1. Design and Optimization of a 24 GHz Microstrip Array Antenna for Non-Contact Vital Sign Monitoring: This study proposes a high-frequency microstrip array antenna design developed in several element configurations (1–5 elements) to improve gain, radiation direction, and sensitivity to micro-movements on the human chest surface. Optimization is performed to ensure performance that meets the requirements of a contactless biomedical radar system.

2. Electromagnetic Validation and Biomedical Safety Evaluation through SAR Analysis: Antenna performance is comprehensively evaluated through electromagnetic simulation using CST Studio Suite, covering key parameters such as reflection coefficient (S_{11}), gain, and radiation pattern. Specific Absorption Rate (SAR) analysis was performed with a multilayer human tissue model (skin, fat, and muscle) to ensure that electromagnetic exposure levels were within safe limits according to international standards.

3. Mechanical Flexibility Analysis: Antenna performance testing under bending conditions was conducted to assess electrical characteristic stability and structural integrity when applied to or near the human body. The analysis results show that the proposed antenna has high flexibility and adequate reliability for integration.

This article is organized as follows. Section 2 presents the proposed system and antenna design, including a single element, two-element array, three-element array, four-element array, and five-element array. Section 3 discusses the simulation results, bending antenna, SAR (Specific Absorption Rate) analysis, and measurement results. Last, Section 4 is the conclusion.

2. METODOLOGY

2.1. Proposed System for Vital Sign Detection

Doppler radar-based vital sign monitoring systems generally use two antennas, a transmit antenna (Tx) and a receive antenna (Rx), to detect micro-movements in the chest area resulting from breathing and heartbeat activity. The Tx antenna transmits electromagnetic waves toward the subject's chest, while the Rx antenna captures the reflected signal that undergoes phase changes due to the Doppler effect. These phase changes correlate directly with chest movement dynamics, allowing them to be processed to extract breathing rate (BR) and heart rate (HR).

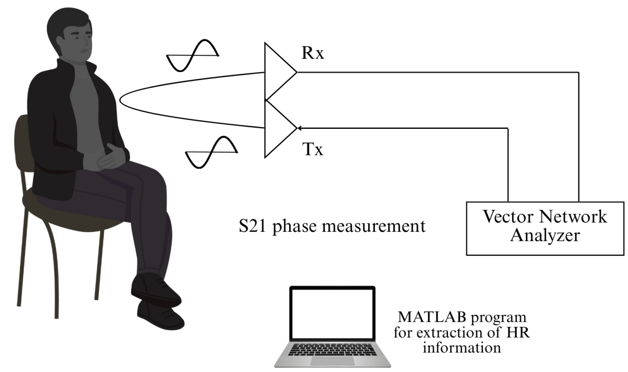

FIGURE 1. S_{21} phase measurement setup to evaluate antenna performance in Doppler radar based vital sign monitoring configurations.

In this study, antenna characterization was performed using a VNA to obtain the S_{21} parameter as part of the evaluation of the antenna's integration potential with the Doppler radar system (Fig. 1). The S_{21} measurement describes the transmission performance between two antennas in static conditions and is not intended as a direct demonstration of vital sign measurement. An explanation of the signal processing stages (filtering, FFT, and peak detection) is provided as a general description of the signal processing flow in Doppler radar applications according to [19], in order to demonstrate the suitability of the antenna design with the requirements of a non-contact vital sign monitoring system.

2.2. Antenna Design

Figure 2 shows the overview of the research methodology, starting from the initial design of the antenna geometry to the final performance evaluation stage. The process begins with

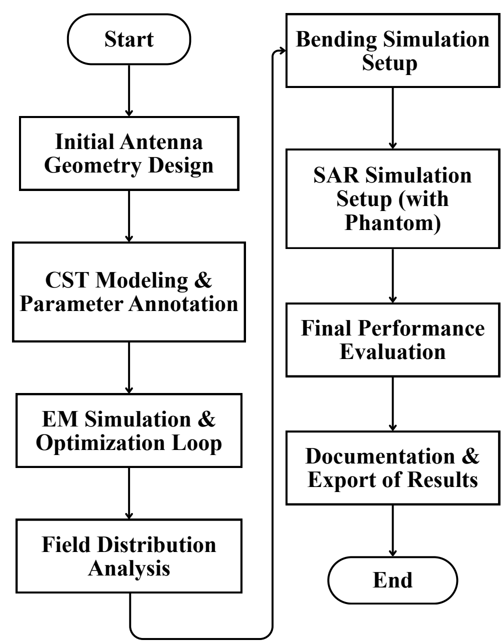

FIGURE 2. Flowchart of the antenna design, simulation, and evaluation process used in this study.

TABLE 1. Antenna parameters.

Parameter	Size (mm)	Parameter	Size (mm)	Parameter	Size (mm)	Parameter	Size (mm)	Parameter	Size (mm)
Lp	26	Wp	22	d	6	$f1$	1	$f2$	1.4
$f3$	0.8	$f4$	1.2	$f5$	1.2	$f6$	2	$g1$	2
$g2$	4.25	$g3$	13	$g4$	4	$g5$	2	$g6$	8
$g7$	2	$g8$	5	$g9$	7	$j1$	7.2	$j2$	1.5
$j3$	6.7	$j4$	2.5	h	0.78				

determining an antenna geometry based on the required operating frequency, continued with antenna modeling in CST Studio Suite with annotations of the parameters to be analyzed. After that, electromagnetic simulation and iterative optimization processes are performed to obtain the desired performance. Field distribution analysis is performed to verify the radiation pattern and electromagnetic response of the antenna. The research flow then continues with bending condition simulations to evaluate the effect of mechanical deformation, followed by SAR simulations using phantoms to evaluate radiation safety aspects. In the final stage, all results are comprehensively analyzed, documented, and exported as research output.

The antenna is designed to work at a frequency of 24 GHz with an input impedance of 50 Ω. The antenna uses a Rogers RT5880 substrate with a substrate dimension of 26 × 22 mm with a thickness (h) of 0.78 mm. The material was chosen because it has a dielectric constant of $(\varepsilon_r) = 2.2$ and a loss tangent of 0.0009, making it ideal for high-frequency applications. The antenna structure consists of three layers, a ground plane at the bottom with a width half that of the substrate, a substrate layer in the middle, and a circular patch and microstrip feed line at the top. The dimensions of the circular patch are determined using the microstrip circular patch antenna design equation [23] to achieve a frequency of 24 GHz, while the microstrip feed line is designed to have a characteristic impedance of 50 Ω to ensure good impedance matching with the radar system. This design has been optimized through electromagnetic simulation to minimize losses and improve radiation efficiency at the target frequency. In addition, the compact geometric configuration allows this antenna to be easily integrated into small radar devices or millimeter wave-based sensor systems.

$$a = \left[\frac{F}{1 + \frac{2h}{\pi F \varepsilon_r}\left(\ln\left(\frac{\pi F}{2h}\right) + 1.7726\right)}\right]^{0.5} \quad (1)$$

where:

$$F = \frac{8.791 \times 10^9}{f_r \sqrt{\varepsilon_r}} \quad (2)$$

In the above equation, a is the radius of the circular patch, h the thickness of the substrate, ε_r the dielectric constant of the substrate used, and f_r the resonance frequency targeted in the antenna design. These four parameters play an important role in determining the physical dimensions of the patch so that the antenna can resonate well at an operating frequency of 24 GHz.

The design of this antenna starts with a single element (Fig. 3(a)) that uses a 6 mm diameter circular patch as the main radiator, connected to a microstrip feed line that has two segments with different widths and lengths to match the impedance and maximize power transfer. The antenna arrays with two elements (Fig. 3(b)), three elements (Fig. 3(c)), four elements (Fig. 3(d)), and five elements (Fig. 3(e)) were developed by adding circular patch elements connected by branched microstrip transmission lines to improve performance. For information, the substrate and ground plane dimensions proposed for the five designs are the same as those shown in Fig. 3(f). Fig. 3(g) shows a perspective view of the proposed antenna. Then, the dimensions for each of the proposed parameters can be seen in Table 1.

The distance between elements and the dimensions of the feed network ($g1$–$g9$) and ($j1$–$j4$) are determined through a parametric simulation-based optimization process. Each parameter is systematically varied to identify the configuration that provides the most optimal impedance matching and radiation pattern with minimal sidelobes.

3. RESULT AND DISCUSSION

3.1. Antenna Parameter Simulation Result

The reflection coefficient (S_{11}) is used to assess the impedance matching between the antenna and the transmission line. The antenna is considered to operate well in the frequency range where $(S_{11}) < 10$ dB, which is the reference for determining the operating bandwidth. Fig. 4(a) shows the S_{11} simulation results for five antenna configurations. The target operating frequency is 24 GHz, but each configuration shows a slightly shifted resonance frequency due to the coupling effect between elements and dimensional optimization.

The single-element antenna has an S_{11} value of -3.96 dB at 24 GHz, but reaches -13 dB at a resonance frequency of 28.472 GHz, with a bandwidth of 5.675 GHz (24.325 GHz–30 GHz). The two-element configuration shows $S_{11} = -10.57$ dB at 24 GHz and -14.73 dB at 23.312 GHz, with a bandwidth of 1.505 GHz (22.575 GHz–24.079 GHz). The three-element configuration shows $S_{11} = -4.71$ dB at 24 GHz, but -14.65 dB at 25.624 GHz, with a bandwidth of 1.639 GHz (24.921 GHz–26.56 GHz). The four-element configuration shows the best performance with a minimum S_{11} value of -39.27 dB at 24.016 GHz and a bandwidth of 1.355 GHz (23.372 GHz–24.727 GHz). Meanwhile, the five-element configuration has $S_{11} = -2.92$ dB at 24 GHz

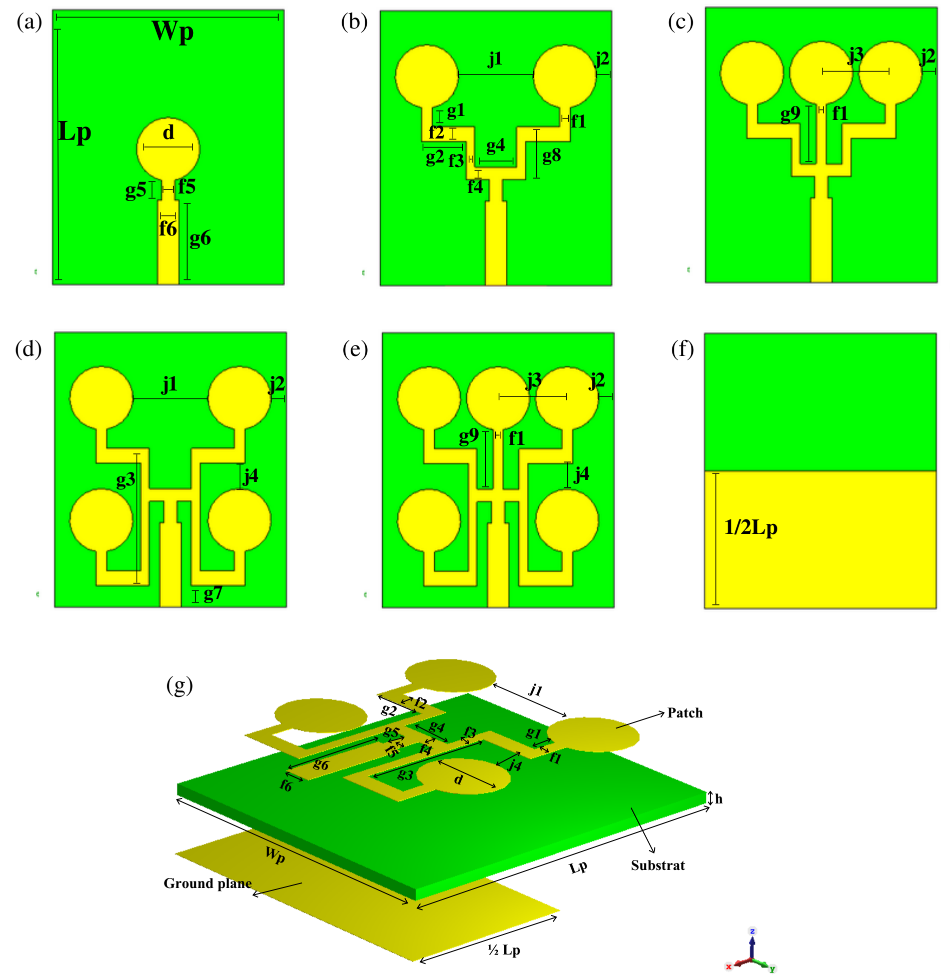

FIGURE 3. The design of the antenna. (a) Single element. (b) Two-element array. (c) Three-element array. (d) Four-element array. (e) Five-element array. (f) Back view of the antenna design. (g) Perspective view of the proposed antenna.

TABLE 2. Quantitative radiation parameters at a frequency of 24 GHz and minimum S_{11}.

Configuration	Plane	HPBW (°)	SLL (dB)	Directivity (dBi)	Main lobe direction (°)	F/B Ratio (dB)	Effc (%)	Minimum S_{11} (dB)
Single element	$\phi = 0°$	112.0	−3.4	3.16	154	6.4	94.2	−13 at 28.472 GHz
	$\phi = 90°$	96.2	−1.2	2.41	116			
Two-element array	$\phi = 0°$	107.5	−1.7	4.51	128	6.5	93.2	−14.73 at 23.312 GHz
	$\phi = 90°$	50.5	N/A	3.03	180			
Three-element array	$\phi = 0°$	62.4	−2.3	4.42	136	10.4	94.4	−14.65 at 25.624 GHz
	$\phi = 90°$	85.9	−3.1	2.96	20			
Four-element array	$\phi = 0°$	41.3	−1.4	5.29	128	6.1	92.5	−39.27 at 24 GHz
	$\phi = 90°$	47.3	−5.3	3.31	180			
Five-element array	$\phi = 0°$	116.0	−1.2	3.61	77	10.9	90.9	−30.52 at 26.016 GHz
	$\phi = 90°$	144.3	−2.5	0.7	12			

and −30.52 dB at 26.016 GHz with a bandwidth of 1.362 GHz (25.381 GHz–26.743 GHz). Based on these results, the four-element configuration was selected as the optimal design because it has the closest resonance frequency to 24 GHz and the best matching value.

Figure 4(b) and Table 2 show that the directivity value of a single antenna is calculated to be 3.16 dBi in the E-plane and 2.41 dBi in the H-plane, indicating a wide radiation pattern. When the antenna is configured into two elements, the directivity increases to 4.51 dBi (E-plane) and 3.03 dBi (H-plane) due

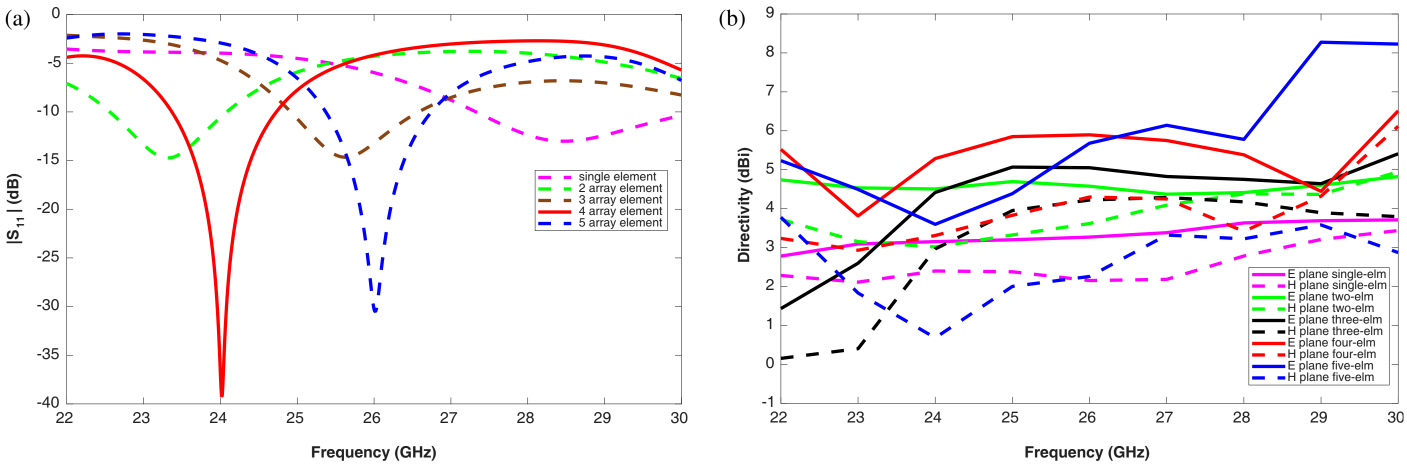

FIGURE 4. Comparison of (a) reflection coefficient, (b) directivity between single-element and multiple-element arrays.

to the strengthening of the radiation field from the combination of two elements. In the three-element configuration, the directivity value decreases slightly to 4.42 dBi and 2.96 dBi, which may be caused by the amplitude imbalance between elements. Furthermore, the four-element configuration produces the highest directivity, at 5.29 dBi in the E-plane and 3.31 dBi in the H-plane, indicating the optimal phase distribution and distance between elements to form a directional beam. However, when the number of elements is increased to five, the directivity actually decreases to 3.61 dBi and 0.7 dBi due to possible phase mismatches between elements that reduce energy concentration in the main direction. These results validate the four-element array design as suitable for 24 GHz radar applications.

Figure 5 shows a comparison of the performance of single antennas with up to five elements in the E plane ($\phi = 0°$) and H plane ($\phi = 90°$). The single antenna shows a wide main lobe with low gain and minimal sidelobes. A gradual increase in the element count results in a narrower main lobe and increased gain, indicating an array gain effect. Starting from the two- to three-element configurations, the radiation pattern becomes more directional, although sidelobes begin to appear due to wave superposition between elements.

Based on Table 2, increasing the element count from one to four significantly narrows the half-power beamwidth (HPBW) from 112° to 41.3° in the E-plane, indicating improved radiation focus and beam efficiency. The main lobe direction is observed to be increasingly stable in the range of 128°–136° for configurations of two to four elements, indicating a similar phase distribution between elements. The side lobe level (SLL) value shows improvement with an increase in the number of elements, especially in the four-element configuration which reaches -5.3 dB in the H-plane, indicating good sidelobe suppression capability. Meanwhile, the front-to-back (F/B) ratio is relatively consistent in the range of 6–10 dB, indicating a balance between forward and backward radiation energy. In the five-element configuration, performance deteriorates, marked by a widening of the HPBW, a shift in the main lobe direction to 77°, and an increase in SLL due to mutual coupling effects and phase mismatch between elements. Overall, the four-element configuration provides the best compromise among radiation focus, sidelobe suppression, and main direction stability, making it most suitable for 24 GHz radar applications in vital sign monitoring.

Based on the simulation results at an operating frequency of 24 GHz, all antenna configurations showed high radiation efficiency, above 90%, confirming that the antenna design has low dielectric and conductor losses, making it suitable for wearable applications. The three-element configuration has the highest efficiency at 94.4%. However, the four-element configuration remains the optimal design in this study because it provides the best balance to support improved sensitivity in detecting micro-movements in vital sign monitoring applications.

Figure 6 shows the surface current distribution at 24 GHz, with blue representing low current and red representing high current. Model 1 shows the current concentration at the center of the antenna. Models 2–5 show a more even and dispersed current distribution as the number of branches increases from two to five, resulting in a wider radiation pattern. Model 5 has the most even current distribution, supporting the widest radiation coverage.

Figure 7 shows the field distribution at a frequency of 24 GHz, which presents a strong resonance pattern, where the E-field reaches a maximum intensity of around 44 kV/m and the H-field around 246 A/m, with the highest energy concentration located in the central region of the structure, indicating that the antenna is operating in its main resonance mode. The decreasing energy distribution towards the edges indicates the effects of conductor boundaries and dielectric attenuation. In general, the symmetrical and high-intensity field distribution pattern in the central part indicates that the antenna is operating close to optimal resonance conditions, while also identifying critical areas relevant to radiation efficiency.

The mutual coupling analysis was not explicitly performed in the array configuration used in this study because the structure only uses one port as a centralized excitation path, so that coupling parameters between elements such as S_{21} or S_{31} cannot be evaluated separately. Nevertheless, the potential for mutual coupling still exists, given the relatively near distance be-

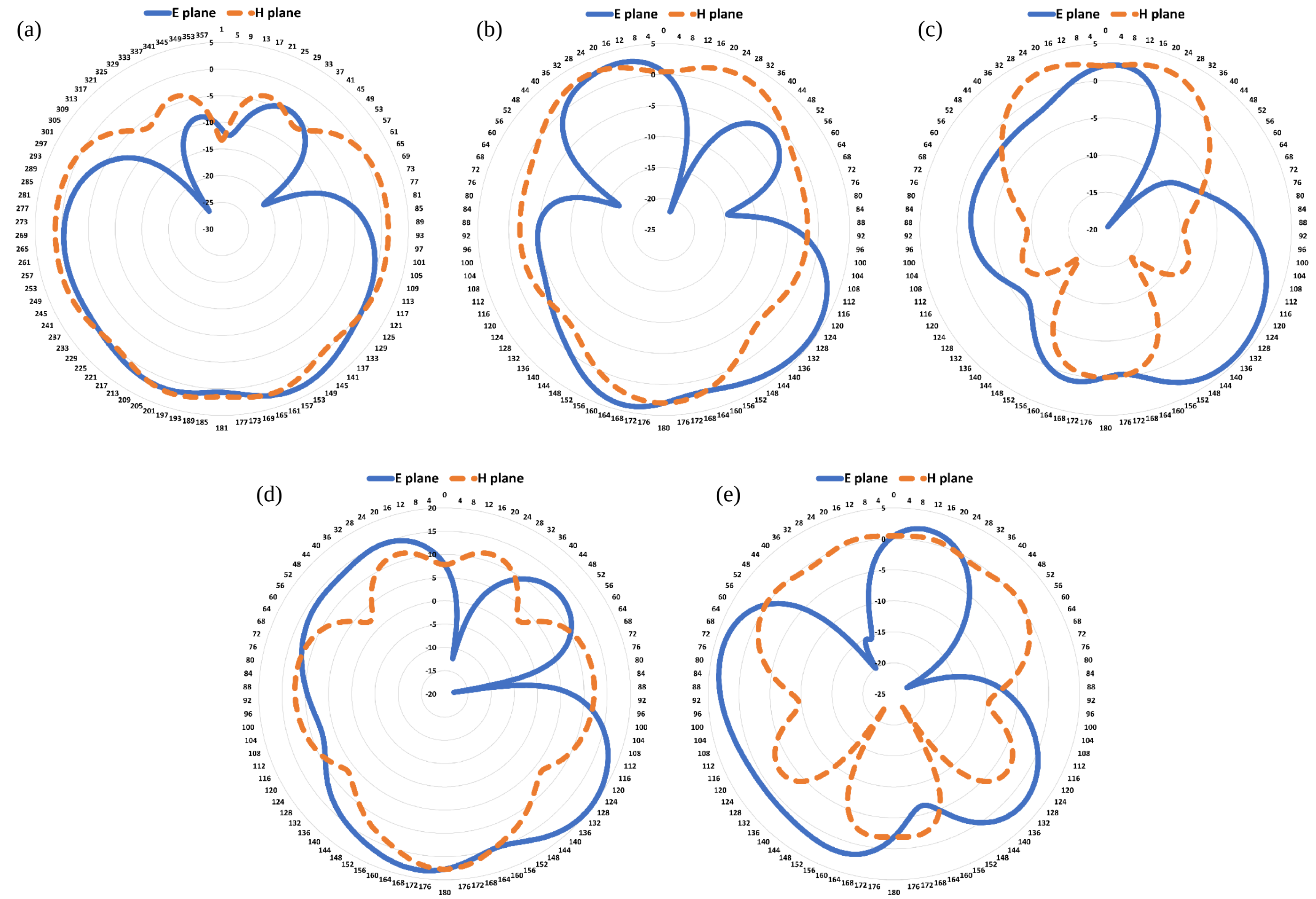

FIGURE 5. Radiation pattern comparison for the E plane ($\phi = 0°$) and H plane ($\phi = 90°$). (a) Single element array. (b) Two-element array. (c) Three-element array. (d) Four-element array. (e) Five-element array.

tween elements at a frequency of 24 GHz, and its effect has been implicitly included in the overall antenna response through the process of impedance matching and radiation pattern optimization. Thus, the resulting performance, including the reflection coefficient, gain, and radiation pattern, represents the array as a whole, even without individual element isolation analysis. Although coupling coefficient analysis cannot be performed on this single-port structure, such a study could be a topic for further development to understand the effects of mutual coupling in more detail.

3.2. Bending Antenna

To evaluate the mechanical flexibility and electromagnetic stability of the designed antenna, bending simulations were performed on four different radius values: 40 mm, 30 mm, 20 mm, and 10 mm, where 10 mm is the condition with the highest bending. The results of the reflection coefficient (S_{11}), directivity, and radiation pattern for each condition are shown in Fig. 8 and Fig. 9 and summarized in Table 3. Visualization of the bending geometry is also shown to indicate the degree of antenna deflection at each bending radius.

The effect of bending on the S_{11} value at 24 GHz shows that changes in geometry shift the antenna's impedance matching conditions. Without bending, the antenna has an S_{11} of -39.27 dB, indicating excellent impedance matching. When the antenna is bent with a radius of 40 mm, the S_{11} value decreases to -20.03 dB. Higher bending at radius 30 mm and 20 mm results in S_{11} values of -18.84 dB and -16.99 dB, indicating a trend of decreasing matching performance as the bending of the structure increases. The condition with the highest bending, at a radius of 10 mm, showed the most significant degradation with an S_{11} value of -12.32 dB. This situation indicates that the more the bend of the antenna is, the more changes occur in current distribution, leading to detuning from the operating frequency.

The antenna directivity in two observation planes ($\phi = 0°$ and $\phi = 90°$) shows that the antenna maintains radiation dominance in the main plane ($\phi = 0°$) under all bending conditions. Under no bending conditions, the directivity reaches 5.29 dBi. When the antenna is bent with radius 40 mm, 30 mm, and 20 mm, the directivity value is in the range of 5.68–5.56 dBi, showing a slight increase due to the cylindrical focusing effect that strengthens the main beam direction. Meanwhile, at the most extreme bending (10 mm radius), the directivity decreases to 4.96 dBi, in line with the decrease in radiation stability due to large structural deformation. These results show that the an-

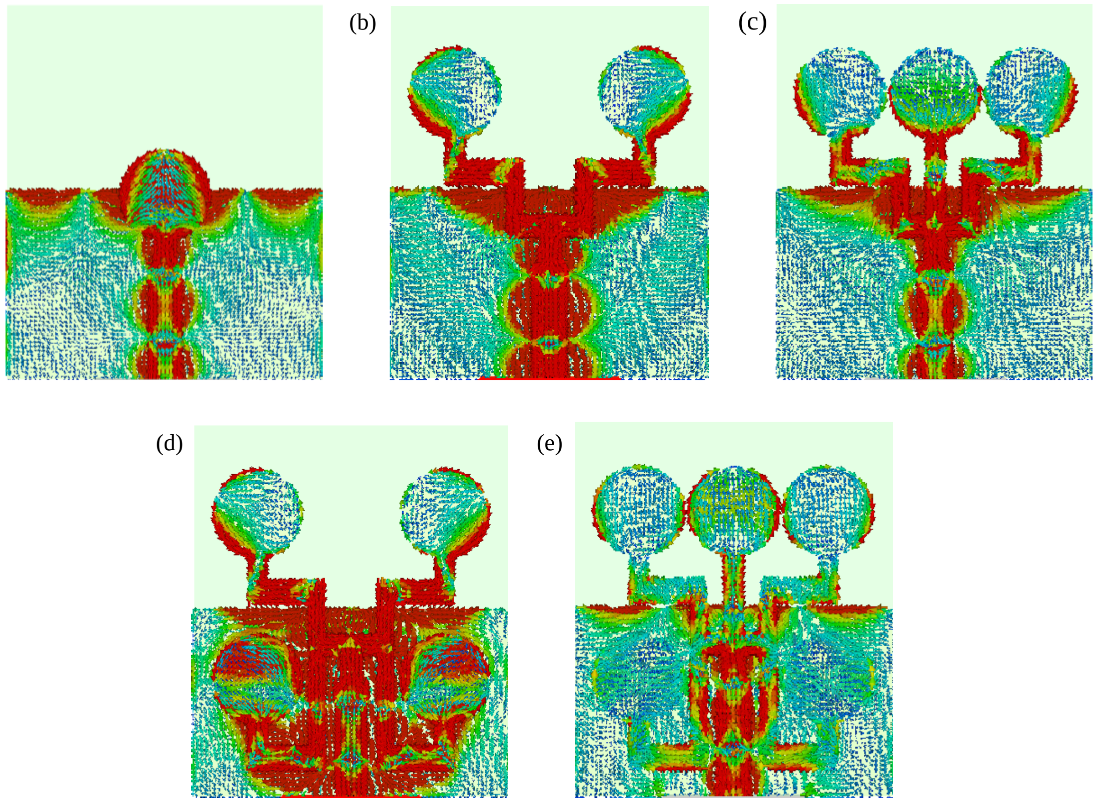

FIGURE 6. Distribution of surface currents. (a) Single element. (b) Two-element array. (c) Three-element array. (d) Four-element array. (e) Five-element array.

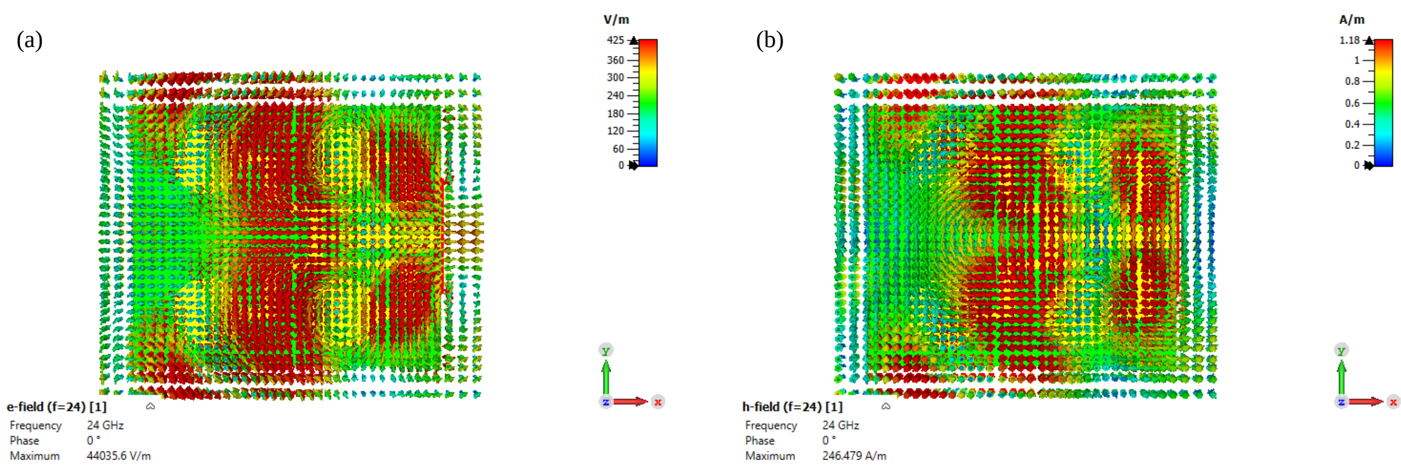

FIGURE 7. (a) E-field distribution at 24 GHz. (b) H-field distribution at 24 GHz.

tenna is still able to maintain the main radiation direction suitable for vital sign radar applications directed at the subject's chest area.

At $\phi = 0°$, the HPBW value is relatively stable in the range of 41–46°, although the SLL is still relatively high (-1.2 to -2.1 dB), indicating a strong sidelobe and possible power loss to the sides. The direction of the main lobe shifts only slightly between 123–128°, with the best F/B ratio shown at a 20 mm bend (8.10 dB), indicating an increase in rear radiation suppression in this configuration. On the other hand, at the $\phi = 90°$ plane, there are more significant differences, especially in HPBW: the 10 mm bend produces a very wide beam spread (145.6°), while the 20 mm bend provides the best radiation focus with a minimum HPBW (39.8°). The SLL values in this plane are also better than those at $\phi = 0°$, ranging from -4.9 to -6.0 dB, while the main lobe direction remains consistent at 180° for all conditions. Furthermore, radiation efficiency tends to decrease with increasing bending, where the condition without bending shows the highest efficiency, and the configuration with a 10 mm radius as the most extreme condition experiences the greatest efficiency degradation due to increased losses and current distribution interference. Overall,

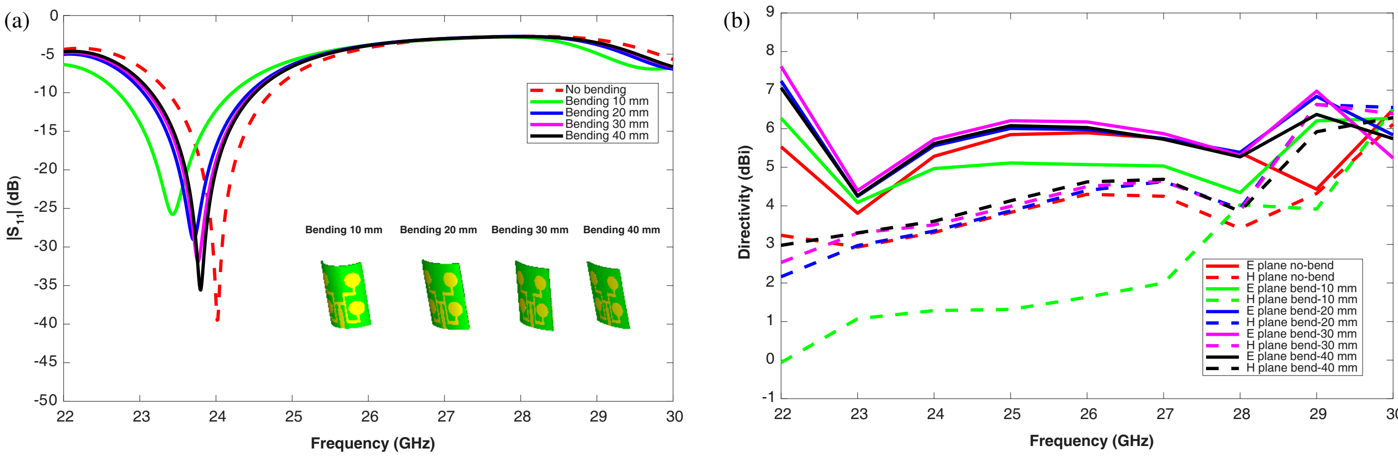

FIGURE 8. Simulation results of (a) S_{11}, (b) directivity of a 24 GHz microstrip antenna under bending conditions of 10 mm, 20 mm, 20 mm and 40 mm.

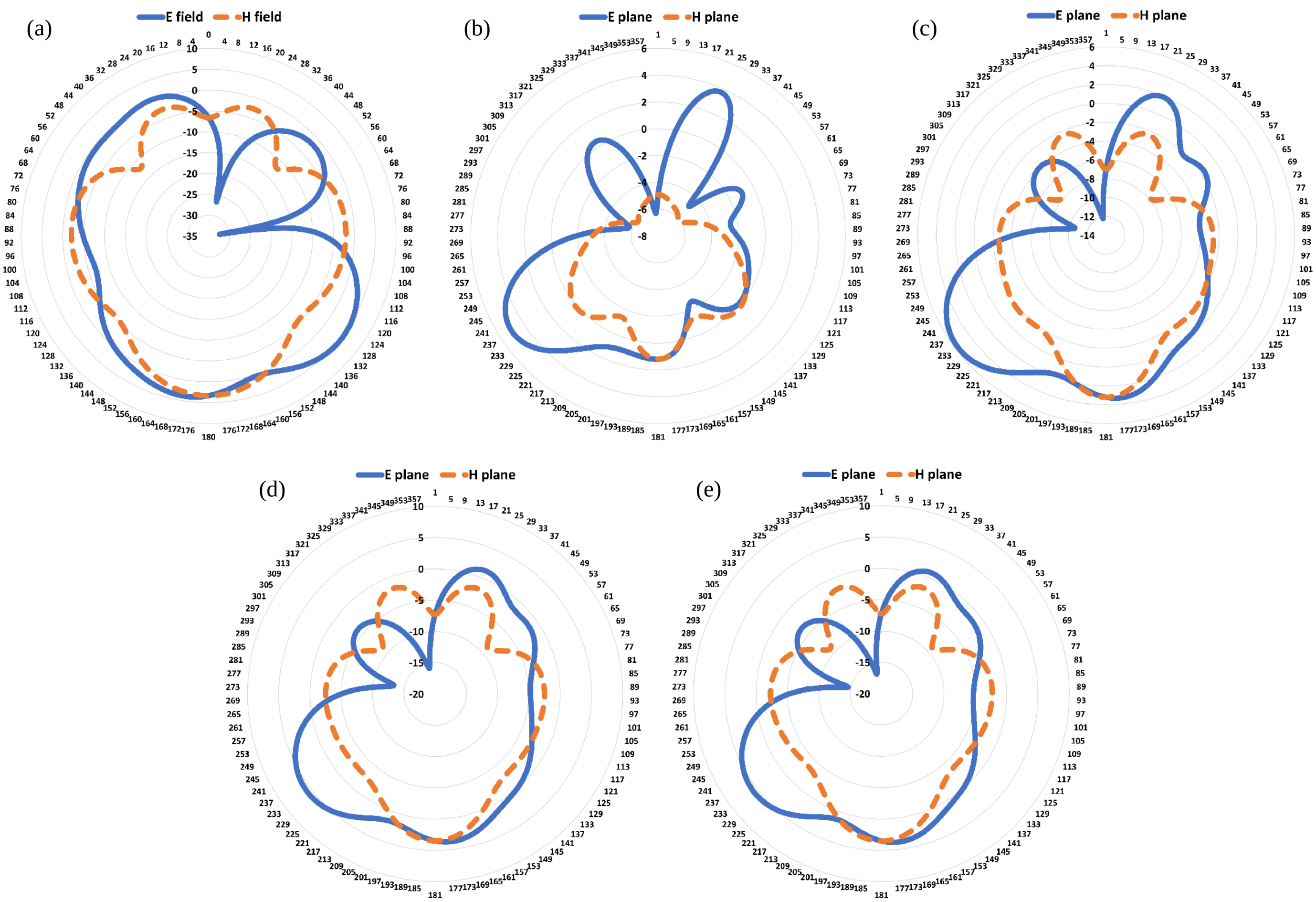

FIGURE 9. Comparison of radiation E plane ($\phi = 0°$) and H plane ($\phi = 90°$). (a) No bending. (b) Bending 10 mm. (c) Bending 20 mm. (d) Bending 30 mm. (e) Bending 40 mm.

different levels of bending produce different characteristics in the antenna's radiation pattern and efficiency, and 20 mm bending can be considered the most balanced configuration because it maintains radiation focus and optimal F/B performance with a controlled decrease in efficiency.

3.3. SAR Analysis

The contact between the antenna and the body can increase the absorption of radio frequency (RF) energy, which could potentially be dangerous to health. In wearable antenna applications, measuring the Specific Absorption Rate (SAR) below safety

TABLE 3. Quantitative radiation parameters for the proposed antenna bending (four-element array) including S_{11} at 24 GHz.

Configuration	Plane	HPBW (°)	SLL (dB)	Directivity (dBi)	Main lobe dir. (°)	F/B (dB)	Effc (%)	S_{11} (dB)
No bending	$\phi = 0°$	41.3	−1.4	5.29	128	6.1	92.5	−39.27
	$\phi = 90°$	47.3	−5.3	3.31	180			
Bending 40 mm	$\phi = 0°$	43.7	−1.7	5.68	128	7.72	92.3	−20.03
	$\phi = 90°$	42.4	−5.7	3.60	180			
Bending 30 mm	$\phi = 0°$	43.8	−2.0	5.72	128	7.6	92.4	−18.84
	$\phi = 90°$	41.5	−5.5	3.51	180			
Bending 20 mm	$\phi = 0°$	46.4	−2.1	5.56	127	8.10	92.3	−16.99
	$\phi = 90°$	39.8	−4.9	3.35	180			
Bending 10 mm	$\phi = 0°$	45.4	−1.2	4.96	123	5.80	92.0	−12.32
	$\phi = 90°$	145.6	−6.0	3.35	180			

TABLE 4. Electrical properties of human tissues.

Tissue	σ (S/m)	ε_r	Loss tan	Density (kg/m^3)	Heat cap. (J/kg·°C)	Therm. cond. (W/m·°C)
Skin	22.841	18.993	0.90073	1109	3391	0.37
Fat	1.4893	3.8361	0.29076	911	2348	0.21
Muscle	29.437	27.395	0.80483	1090	3421	0.49

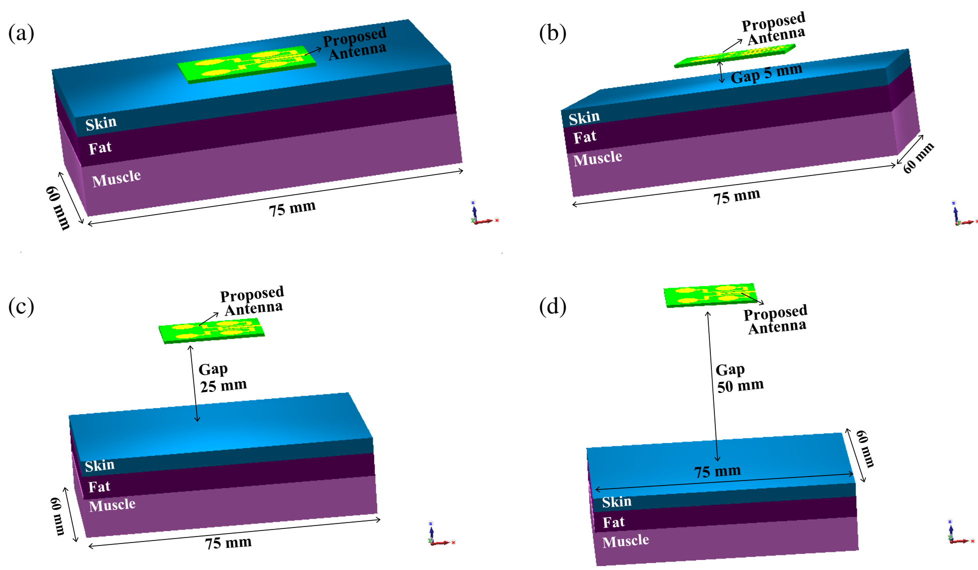

FIGURE 10. SAR simulation setup at different antenna to body distances. (a) 0 mm (on-body). (b) 5 mm. (c) 25 mm. (d) 50 mm.

limits is a main consideration. SAR measures the level of electromagnetic radiation energy absorbed by the human body and is expressed in watts per kilogram (W/Kg) [24].

A three-layer phantom body at a frequency of 24 GHz was designed in CST Studio Suite with the human tissue electrical properties for the skin, fat, and muscle layers. The skin, fat, and muscle layers are 4 mm, 6 mm, and 10 mm thick, respectively. Table 4 describes the electrical properties of the phantom designed based on references from the IT'IS Foundation database, which is used extensively for electromagnetic and SAR-related studies. Fig. 10 shows the SAR simulation setup at the antenna to body distance. In this SAR simulation, an input power of 0.5 mW (−3 dBm) was used. This value was chosen to represent the operating conditions of low-power wearable devices. A previous study [19] reported that vital sign monitoring systems using wearable antennas operate at an RF power of around −3 dBm for BR and HR measurements. Therefore, the use of −3 dBm power in the SAR simulation is a conservative and

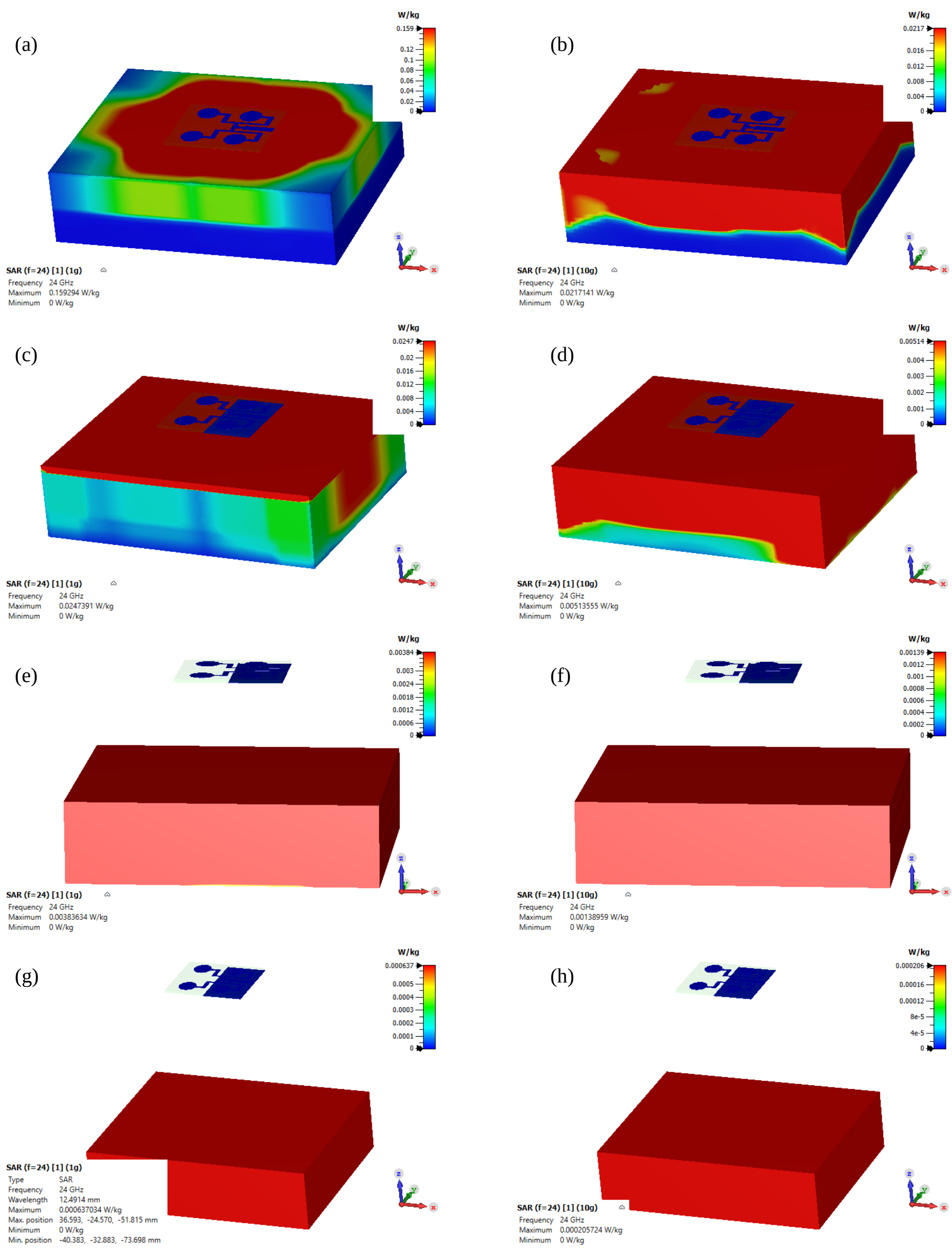

FIGURE 11. SAR. (a) On-body over 1 gram. (b) On-body over 10 gram. (c) 5 mm away from the antenna over 1 gram. (d) 5 mm away from the antenna over 10 gram. (e) 25 mm away from the antenna over 1 gram. (f) 25 mm away from the antenna over 10 gram. (g) 50 mm away from the antenna over 1 gram. (h) 50 mm away from the antenna over 10 gram.

realistic approach to evaluating electromagnetic radiation exposure. The antenna and the body-equivalent phantom were simulated, and SAR values were obtained for 1 g and 10 g of tissue. The SAR estimates for the body analysis are shown in Fig. 11.

The SAR value is obtained by approaching the antenna to the phantom according to the desired test distance. The SAR obtained on the human body for 1 g and 10 g networks is 0.159 W/kg and 0.022 W/kg. Then, several tests were conducted at specific distances, 5 mm from the body, 25 mm from the body, and 50 mm from the body. A change in SAR values was observed at a distance of 5 mm for 1 g and 10 g tissue, which were 0.025 W/kg and 0.005 W/kg. At a distance of 25 mm from the body, the SAR values for 1 g and 10 g of tissue

TABLE 5. Summary of SAR analysis.

SAR	1 g (W/kg)	10 g (W/kg)
On-body	0.159	0.022
5 mm away	0.025	0.005
25 mm away	0.004	0.001
50 mm away	0.0006	0.0002

TABLE 6. Comparison with previous research.

Ref.	Material	Substrate Dimension (mm^3)	Frequency (GHz)	Min S_{11} (dB)	Bandwidth (GHz)	Gain (dBi)	Rad. Effc (%)	Application
[19]	LCP ($\varepsilon_r = 3.35$)	$36.5 \times 53 \times 0.1$	24	-28.75	0.19	5.81	N/A	Vital signs monitoring
[20]	polypropylene (PP) ($\varepsilon_r = 2.2$)	$98.7 \times 14.4 \times 0.52$	24	-25	0.28	16.8	91	Radar imaging application in collision-avoidance systems
[28]	Rogers 5880 ($\varepsilon_r = 2.2$)	$16.19 \times 16.19 \times 0.127$	24	-17	2.75	5.5	N/A	Flexible antenna for 24 GHz ISM WBAN
[29]	RO300 ($\varepsilon_r = 3.0$)	$14.1 \times 9.6 \times 0.762$	24.05–24.25	-30 to -35	3	6.73	97	Wearable electronic travel aid system
[30]	HRSi/SiO_2 ($\varepsilon_r = 3.9/11.7$)	$34.88 \times 25.47 \times 6$	24	-32.5	around 0.5	1.5–4	31–65	Tunable antenna
[31]	RT/duroid 5880 ($\varepsilon_r = 2.2$)	$40 \times 6 \times 0.8$	24	-20	4.44	9.8	87	Radar, communication and sensors applications
[32]	Rogers 5880 ($\varepsilon_r = 2.2$)	around $30 \times 10 \times 0.09$	24	-34.25	0.8	12.7	N/A	D2D applications
[33]	Rogers RO4350B ($\varepsilon_r = 3.48$)	$21 \times 29 \times 0.254$	24	around -36	0.51	10	N/A	Moving target sensing applications
[34]	Rogers RO4003C ($\varepsilon_r = 3.38$)	$65 \times 22 \times 0.813$	24	-23.3	0.4	13.5	N/A	Automotive radar applications
[35]	Rogers RO3003 ($\varepsilon_r = 3$)	$26.7 \times 20.4 \times 0.8$	24	around -38	1.7	9.2	100	Collision avoidance imaging application
Proposed	**Rogers 5880 ($\varepsilon_r = 2.2$)**	**$26 \times 22 \times 0.78$**	**24**	**-39.27**	**1.355**	**5.29**	**92.5**	**Vital signs monitoring**

were 0.004 W/kg and 0.001 W/kg. And at a distance of 50 mm from the body, the SAR values for 1 g and 10 g of tissue were 0.0006 W/kg and 0.0002 W/kg. The summary of the SAR analysis results is shown in Table 5.

The limit for Specific Absorption Rate (SAR) is set at 1.6 W/kg above 1 g by the Federal Communications Commission (FCC) and 2 W/kg above 10 g by the International Commission on Non-Ionizing Radiation Protection (ICNIRP) and IEEE C95.1-2019 [25]. Therefore, from several SAR tests that have been conducted, it can be concluded that antennas are safe to use on or near the body. The use of high frequencies of 24 GHz is very influential because the higher the frequency is used, the greater the electromagnetic waves that can be absorbed by the body are. It can also be concluded that when the RF source is placed far from the body, the SAR value decreases significantly.

3.4. Antenna Measurement Results

Figure 12 shows a comparison of simulation results and measured reflection coefficients (S_{11}) of the antenna after the fabrication process. In the simulation results, the antenna shows a resonance frequency of around 24 GHz with an (S_{11}) value below -30 dB. Meanwhile, the measurement results show resonance that remains at around 24 GHz, but with a minimum (S_{11}) value of around -18 dB. The difference between the simulation results and the S_{11} measurements, which reached around 12 dB, can be explained by several physical factors that commonly occur in flexible antennas, especially at high frequencies such as 24 GHz. One of these factors is the variation in the dielectric properties of the substrate material after the fabrication process. The relative permittivity and thickness of the substrate can change slightly due to heat pressure or stretch-

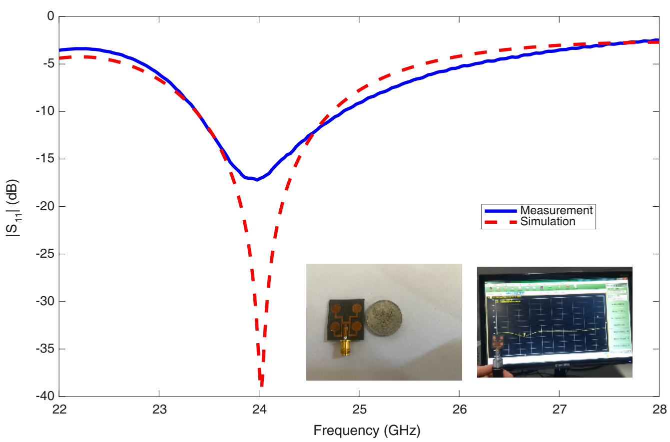

FIGURE 12. A comparison of reflection coefficient (S_{11}) simulation and antenna measurement.

ing during the copper coating process, which can shift the resonance frequency by hundreds of megahertz and affect the S_{11} value by several dB. In addition, imperfections in soldering and SMA connector transitions also contribute to impedance mismatch between the transmission line and the antenna. These factors have been reported in studies [26] and [27]. Despite these differences, the measurement results still show good antenna performance because the reflection coefficient value is below -10 dB at the desired operating frequency. Therefore, the produced antenna can be categorized as suitable for use in applications in the 24 GHz frequency range.

Based on Table 6, the antennas in the previous literature show different characteristics and performance focuses according to their respective application requirements. For the 24 GHz radar-based vital sign monitoring system, the proposed antenna offers a combination of relevant parameters, especially in terms of impedance matching, compact physical size, and structural simplicity. This antenna shows the best impedance matching performance with an S_{11} value of -39.27 dB, which is a lower value than all references [19] to [35], and ensures high power transfer efficiency without requiring a multi-level structure or complex coupling techniques. The antenna dimensions ($26 \times 22 \times 0.78\,\text{mm}^3$) are not the smallest, but it can still be categorized as a compact design and takes advantage of a single patch configuration on a Rogers 5880 substrate, making the fabrication process easier than antennas that use layered substrates or special materials such as ultra-thin LCP or SiO_2. In addition, the proposed design has a fairly wide bandwidth (1.355 GHz), which contributes to the stability of radar operation under varying environmental conditions. Although some references offer higher directivity, the directivity value of 5.29 dBi in this design is suitable for short-range applications such as respiratory and heart rate monitoring, which do not require high gain. Meanwhile, the radiation efficiency of 92.5% indicates that the antenna is capable of maintaining good radiation performance despite its simple structure. Therefore, the proposed design provides a suitable combination of matching performance, compact size, structural simplicity, adequate bandwidth, and sufficient gain for a 24 GHz vital sign monitoring radar system.

4. CONCLUSION

A compact and efficient 24 GHz microstrip array antenna has been successfully designed and analyzed for non-contact vital sign detection. Simulation and measurement results show that the four-element array configuration provides the best impedance matching (-39.27 dB), stable gain (5.29 dBi), and directional radiation pattern at the target frequency. SAR analysis confirms that the antenna is safe for use near or in contact with the human body in accordance with ICNIRP and FCC safety standards. Additionally, bending performance evaluation shows the antenna remains electrically stable even under curved conditions, highlighting its suitability for wearable and flexible biomedical systems. These findings confirm that the proposed antenna design is a promising candidate for compact, low-cost, and safe health-based radar applications, enabling accurate and comfortable long-term vital sign monitoring.

ACKNOWLEDGEMENT

This research was partially funded by the Indonesia Collaboration Research Funding from Legal-Entity State Higher Education Institutions (Universitas Negeri Surabaya, Universitas Indonesia, and Universitas Hasanuddin); and partially by Riset Kolaborasi Indonesia (RKI), Universitas Negeri Surabaya (Indonesia), under contract Grant No. B/52732/UN38.III.1/LK.04.00/2025.

REFERENCES

[1] Alzahrani, M. S., A. H. Albishi, A. E. Alfaifi, A. M. Alzahrani, R. I. Aldoosary, S. Y. Alshabeeb, A. A. Alammar, B. M. Alalrashidi, E. M. Zoqeei, and O. A. Kofiyah, "Vital signs role and significance in detecting early cardiac events," *International Journal of Community Medicine And Public Health*, Vol. 11, No. 1, 419–423, Dec. 2023.

[2] Yu, Y., B. Jain, G. Anand, M. Heidarian, A. Lowe, and A. Kalra, "Technologies for non-invasive physiological sensing: Status, challenges, and future horizons," *Biosensors and Bioelectronics: X*, Vol. 16, 100420, 2024.

[3] Shuzan, M. N. I., M. H. Chowdhury, M. S. Hossain, M. E. H. Chowdhury, M. B. I. Reaz, M. M. Uddin, A. Khandakar, Z. B. Mahbub, and S. H. M. Ali, "A novel non-invasive estimation of respiration rate from motion corrupted photoplethysmograph signal using machine learning model," *IEEE Access*, Vol. 9, 96 775–96 790, 2021.

[4] Tiwari, S., A. Jain, A. K. Sharma, and K. M. Almustafa, "Phonocardiogram signal based multi-class cardiac diagnostic decision support system," *IEEE Access*, Vol. 9, 110 710–110 722, 2021.

[5] Ghosh, S., B. P. Chattopadhyay, R. M. Roy, J. Mukherjee, and M. Mahadevappa, "Non-invasive cuffless blood pressure and heart rate monitoring using impedance cardiography," *Intelligent Medicine*, Vol. 2, No. 04, 199–208, 2022.

[6] Li, S., L. Zhao, B. Zhang, Y. Yuan, H. Cao, and Z. Yu, "Ultrasound cardiogram-based diagnosis of cardiac hypertrophy from hypertension and analysis of its relationship with expression of autophagy-related protein," *Annals of Palliative Medicine*, Vol. 11, No. 2, 68 494–68 694, 2022.

[7] Xu, H., M. P. Ebrahim, K. Hasan, F. Heydari, P. Howley, and M. R. Yuce, "Accurate heart rate and respiration rate detection based on a higher-order harmonics peak selection method using radar non-contact sensors," *Sensors*, Vol. 22, No. 1, 83, 2022.

[8] Shan, J., K. Rambabu, Y. Zhang, and J. Lin, "High gain array antenna for 24 GHz FMCW automotive radars," *AEU — International Journal of Electronics and Communications*, Vol. 147, 154144, 2022.

[9] Arasteh, E., E. S. Veldhoen, X. Long, M. van Poppel, M. van der Linden, T. Alderliesten, J. Nijman, R. de Goederen, and J. Dudink, "Ultra-wideband radar for simultaneous and unobtrusive monitoring of respiratory and heart rates in early childhood: A deep transfer learning approach," *Sensors*, Vol. 23, No. 18, 7665, 2023.

[10] Antolinos, E. and J. Grajal, "Comprehensive comparison of continuous-wave and linear-frequency-modulated continuous-wave radars for short-range vital sign monitoring," *IEEE Transactions on Biomedical Circuits and Systems*, Vol. 17, No. 2, 229–245, 2023.

[11] Tzou, S.-J., I.-H. Chen, T.-H. Chu, D.-M. Chian, F.-K. Wang, Y.-K. Lee, and C.-Y. Ko, "Accuracy of self-injection locking radar system for vital signs detection during the COVID-19 pandemic at a hospital in taiwan: Measuring vital signs accurately with sil radar for hospital healthcare," *Medical Science Monitor*, Vol. 29, e939949, 2023.

[12] Turppa, E., J. M. Kortelainen, O. Antropov, and T. Kiuru, "Vital sign monitoring using FMCW radar in various sleeping scenarios," *Sensors*, Vol. 20, No. 22, 6505, 2020.

[13] Vignoli, E., P. D. Viesti, and G. M. Vitetta, "A deterministic method for contactless monitoring of vital signs using multiple FMCW radars in the 24 GHz band," *IEEE Access*, Vol. 13, 27 868–27 892, 2025.

[14] Seflek, I., Y. E. Acar, and E. Yaldiz, "Small motion detection and non-contact vital signs monitoring with continuous wave doppler radars," *Elektronika ir Elektrotechnika*, Vol. 26, No. 3, 54–60, 2020.

[15] Cupal, M. and Z. Raida, "Slot antennas integrated into 3D knitted fabrics: 5.8 GHz and 24 GHz ISM bands," *Sensors*, Vol. 22, No. 7, 2707, 2022.

[16] Khan, F. and S. H. Cho, "A detailed algorithm for vital sign monitoring of a stationary/non-stationary human through IR-UWB radar," *Sensors*, Vol. 17, No. 2, 290, 2017.

[17] Nurhayati, N., F. Y. Zulkifli, A. H. Rombe, R. A. Firdaus, M. F. E. Purnomo, M. T. Le, and A. J. A. Al-Gburi, "Design and studies of monopole antenna integrated with metamaterial-based CSRR and rectangular spiral shaped for super wide band application," *Results in Engineering*, Vol. 26, 105459, 2025.

[18] Sobrinho, R. E. F., A. M. de Oliveira, A. M. de oliveira Neto, A. J. R. Serres, A. R. de Alexandria, Filho, M. B. Perotoni, N. Nurhayati, and I. C. Nogueira, "Vivaldi antipodal antenna with high gain and reduced side lobe level using slot edge with new neogothic fractal by cantor with application in medical images for tumor detection," *INAJEEE (Indonesian Journal of Electrical and Electronics Engineering)*, Vol. 3, No. 1, 25–31, 2020.

[19] Kathuria, N. and B.-C. Seet, "24 GHz flexible antenna for doppler radar-based human vital signs monitoring," *Sensors*, Vol. 21, No. 11, 3737, 2021.

[20] De Cos Gómez, M. E., H. F. Álvarez, and F. L.-H. Andrés, "PP-based 24 GHz wearable antenna," *Wireless Networks*, Vol. 30, No. 2, 867–882, 2024.

[21] Chen, P.-Y., H.-Y. Lin, Z.-H. Zhong, N.-S. Pai, C.-M. Li, and C.-H. Lin, "Contactless and short-range vital signs detection with doppler radar millimetre-wave (76–81 GHz) sensing firmware," *Healthcare Technology Letters*, Vol. 11, No. 6, 427–436, 2024.

[22] Nurhayati, N., A. N. D. N. Fahmi, P. Puspitaningayu, O. Wiriawan, B. Raafi'u, F. A. Iskandarianto, A. J. A. Al-Gburi, A. Varshney, and S. Johari, "Wearable wideband textile coplanar vivaldi antenna for medical and IoT application," *Progress In Electromagnetics Research C*, Vol. 148, 145–156, 2024.

[23] Djouimaa, A. and K. Bencherif, "Design of a compact circular microstrip patch antenna for 5G applications," *Engineering, Technology & Applied Science Research*, Vol. 14, No. 4, 16 020–16 024, Aug. 2024.

[24] Karad, K. V., V. S. Hendre, J. L. Rajput, V. Kadam, V. E. Narawade, R. Bakale, and G. D. Londhe, "A SAR analysis of hexagonal-shaped UWB antenna for healthcare applications," *EURASIP Journal on Wireless Communications and Networking*, Vol. 2024, No. 1, 72, 2024.

[25] Hashim, F. F., W. N. L. B. W. Mahadi, T. B. A. Latef, and M. B. Othman, "Fabric-metal barrier for low specific absorption rate and wide-band felt substrate antenna for medical and 5G applications," *Electronics*, Vol. 12, No. 12, 2754, 2023.

[26] Lu, S., K. J. Nicholson, J. Patniotis, J. Wang, and W. K. Chiu, "The effects of mechanical loading on resonant response of a conformal load-bearing antenna system," *Sensors*, Vol. 24, No. 19, 6206, 2024.

[27] Riener, C., T. Bauernfeind, S. Kvasnicka, K. Roppert, H. Hackl, and M. Kaltenbacher, "Numerical investigation of signal launch imperfections for edge mount RF connectors," *Electronics*, Vol. 11, No. 13, 1990, 2022.

[28] Ali, M., J. C. Batchelor, I. Ullah, and N. J. Gomes, "Ultra-thin EBG backed flexible antenna for 24 GHz ISM band WBAN," in *2022 Antenna Measurement Techniques Association Symposium (AMTA)*, 1–4, Denver, CO, USA, 2022.

[29] Berdasco, A. F., M. E. de Cos Gómez, J. Laviada, and F. Las-Heras, "AMC-backed twin arrow antenna for wearable electronic travel aid system at 24 GHz," *IEEE Antennas and Wireless Propagation Letters*, Vol. 23, No. 11, 3337–3341, 2024.

[30] Aldrigo, M., M. Dragoman, S. Iordanescu, A. Avram, O.-G. Simionescu, C. Parvulescu, H. E. Ghannudi, S. Montori, L. Nicchi, S. Xavier, and A. Ziaei, "Tunable 24-GHz antenna arrays based on nanocrystalline graphite," *IEEE Access*, Vol. 9, 122 443–122 456, 2021.

[31] Sharma, M., A. K. Gautam, N. Agrawal, and N. Singh, "Design of MIMO planar antenna at 24 GHz band for radar, communication and sensors applications," *AEU — International Journal of Electronics and Communications*, Vol. 136, 153747, 2021.

[32] Kakaraparty, K. and I. Mahbub, "Design and performance analysis of a 24 GHz series-fed 1 × 5 antenna array with material deformation for D2D applications," in *2023 IEEE International Symposium on Antennas and Propagation and USNC-URSI Radio Science Meeting (USNC-URSI)*, 1575–1576, Portland, OR, USA, 2023.

[33] Kim, S., D. K. Kim, Y. Kim, J. Choi, and K.-Y. Jung, "A 24 GHz ISM-band doppler radar antenna with high isolation characteristic for moving target sensing applications," *IEEE Antennas and Wireless Propagation Letters*, Vol. 18, No. 7, 1532–1536, 2019.

[34] Yu, C.-A., K.-S. Chin, and R. Lu, "24-GHz wide-beam patch antenna array laterally loaded with parasitic strips," in *2019 Cross Strait Quad-Regional Radio Science and Wireless Technology Conference (CSQRWC)*, 1–3, Taiyuan, China, 2019.

[35] Flórez Berdasco, A., M. E. de Cos Gómez, H. F. Álvarez, and F. Las-Heras, "Millimeter wave array-HIS antenna for imaging applications," *Applied Physics A*, Vol. 129, No. 6, 397, 2023.